

Cross-scale interaction of host tree size and climatic water deficit governs bark beetle-induced tree mortality

Michael J. Koontz^{1,2,3*}, Andrew M. Latimer^{1,2}, Leif A. Mortenson⁴, Christopher J. Fettig⁵, Malcolm P. North^{1,2,6}

¹Graduate Group in Ecology, University of California, Davis, CA, USA

²Department of Plant Sciences, University of California, Davis, CA, USA

³Earth Lab, University of Colorado-Boulder; Boulder, CO, USA

⁴USDA Forest Service, Pacific Southwest Research Station, Placerville, CA, USA

⁵USDA Forest Service, Pacific Southwest Research Station, Davis, CA, USA

⁶USDA Forest Service, Pacific Southwest Research Station, Mammoth Lakes, CA, USA

*Correspondence: michael.koontz@colorado.edu

Keywords: *Dendroctonus brevicomis*, disturbance, drones, *Pinus ponderosa*, Sierra Nevada, structure from motion, forest structure, climate change-type drought, macroecology, Gaussian process

Abstract word count: 387

Overall .docx word count: 13619

Main text word count: 4786 (Intro: 1566; Results: 456 (45+140+361); Discussion: 2764)

Methods word count: 3493 (734+642+1720+397)

Text boxes word count: 0

Date report generated: November 04, 2020

Abstract

The recent Californian hot drought (2012-2016) precipitated unprecedented ponderosa pine (*Pinus ponderosa*) mortality, largely attributable to the western pine beetle (*Dendroctonus brevicomis*; WPB). Broad-scale climate conditions can directly shape tree mortality patterns, but mortality rates respond non-linearly to climate when local-scale forest characteristics influence the behavior of tree-killing bark beetles (e.g., WPB). To test for these cross-scale interactions, we conduct aerial drone surveys at 32 sites along a gradient of climatic water deficit (CWD) spanning 350 km of latitude and 1000 m of elevation in WPB-impacted Sierra Nevada forests. We map, measure, and classify over 450,000 trees within 9 km², validating measurements with coincident field plots. We find greater size, proportion, and density of ponderosa pine (the WPB host) increase host mortality rates, as does greater CWD. Critically, we find a CWD/host size interaction such that larger

30 trees amplify host mortality rates in hot/dry sites. Management strategies for climate change adaptation
31 should consider how bark beetle disturbances can depend on cross-scale interactions, which challenge our
32 ability to predict and understand patterns of tree mortality.

33 **Introduction**

34 Bark beetles dealt the final blow to many of the nearly 150 million trees killed in the California hot drought
35 of 2012 to 2016 and its aftermath.¹ A harbinger of climate change effects to come, record high temperatures
36 exacerbated the drought,^{2,3} which increased water stress in trees,^{4,5} making them more susceptible to
37 colonization by bark beetles.^{6,7} Further, a century of fire suppression has enabled forests to grow into dense
38 stands, which can also make them more vulnerable to bark beetles.^{6,8,9} This combination of environmental
39 conditions and forest structural characteristics led to tree mortality events of unprecedented size across the
40 state.^{10,11}

41 Tree mortality exhibited a strong latitudinal and elevational gradient^{4,11} that can only be partially explained
42 by coarse-scale measures of environmental conditions (i.e., historic climatic water deficit; CWD) and current
43 forest structure (i.e., current regional basal area).¹¹ Progressive loss of canopy water content offers additional
44 insight into tree stress and mortality risk, but cannot ultimately resolve which trees are actually killed by
45 bark beetles or elucidate factors driving bark beetle population dynamics and spread.⁵ Bark beetles respond
46 to local forest characteristics in positive feedbacks that non-linearly alter tree mortality dynamics against a
47 background of environmental conditions that stress trees.^{12,13} Thus, an explicit consideration of local forest
48 structure and composition^{14,15} as well as its cross-scale interaction with regional climate conditions¹⁶ can
49 refine our understanding of tree mortality patterns from California's recent hot drought. The challenge of
50 simultaneously measuring the effects of both local-scale forest features (such as structure and composition)
51 and broad-scale environmental conditions (e.g., CWD) on forest insect disturbance leaves their interaction
52 effect relatively underexplored.¹⁴⁻¹⁷

53 The ponderosa pine/mixed-conifer forests in California's Sierra Nevada region are characterized by regular bark
54 beetle disturbances, primarily by the influence of western pine beetle (*Dendroctonus brevicomis*; WPB) on its
55 host ponderosa pine (*Pinus ponderosa*).¹⁸ WPB is a primary bark beetle—its reproductive success is contingent
56 upon host tree mortality, which itself requires enough beetles to mass attack the host tree and overwhelm its
57 defenses.¹⁹ This Allee effect creates a strong coupling between beetle selection behavior of host trees and
58 host tree susceptibility to colonization.¹⁹⁻²¹ A key defense mechanism of conifers to bark beetle attack is to
59 flood beetle bore holes with resin, which physically expels colonizing beetles, can be toxic to the colonizers
60 and their fungi, and may interrupt beetle communication.^{22,23} Under normal conditions, weakened trees

61 with compromised defenses are the most susceptible to colonization and will be the main targets of primary
62 bark beetles like WPB.^{13,23,24} Under severe water stress however, many trees no longer have the resources
63 available to mount a defense.^{7,13} Drought,^{12,25–27} especially when paired with high temperatures,^{24,28–30} can
64 trigger increased bark beetle-induced tree mortality as average tree vigor declines. As the local population
65 density of beetles increases due to successful reproduction within spatially-aggregated susceptible trees, mass
66 attacks grow in size and become capable of overwhelming formidable tree defenses. Even large healthy trees
67 may be susceptible to colonization and mortality when beetle population density is high.^{13,23,24} Thus, water
68 stress and beetle population density interact to influence whether individual trees are susceptible to bark
69 beetles. When extreme or prolonged drought increases host tree vulnerability, bark beetle population growth
70 rates increase, then become self-amplifying as greater beetle densities make additional host trees prone to
71 successful mass attack.^{12,13,15,24}

72 WPB activity is strongly influenced by forest structure– the spatial arrangement and size distribution of trees–
73 and tree species composition. Taking forest structure alone, high-density forests are more prone to bark
74 beetle-induced tree mortality compared to thinned forests^{6,9} which may arise as greater competition for water
75 resources amongst crowded trees lowers average tree resistance,³¹ or because smaller gaps between trees protect
76 pheromone plumes from dissipation by the wind and thus enhance intraspecific beetle communication.³² Tree
77 size is another aspect of forest structure that affects bark beetle host selection behavior with smaller trees
78 tending to have lower capacity for resisting attack, but larger trees being more desirable targets on account
79 of their thicker phloem providing greater nutritional content.^{13,33–35} Throughout an outbreak, some bark
80 beetle species will collectively “switch” the preferred size of tree to attack in order to navigate this trade-off
81 between host susceptibility and host quality.^{13,21,36–39} Taking forest composition alone, WPB activity in the
82 Sierra Nevada mountain range of California is necessarily tied to the regional distribution of its exclusive host,
83 ponderosa pine.¹⁸ Colonization by primary bark beetles can also depend on the local relative frequencies of
84 tree species in forest stands, reflecting the more general pattern that specialist insect herbivory tends to be
85 lower in taxonomically diverse forests compared to monocultures.^{40,41}

86 The interaction between forest structure and composition at both stand- and tree- scales also drives WPB
87 activity. For instance, dense forest stands with high host availability may experience greater beetle-induced
88 tree mortality because dispersal distances between potential host trees are shorter, which reduces predation
89 of adults searching for hosts and facilitates higher rates of colonization.^{33,42,43} High host availability can also
90 reduce the chance of individual beetles wasting their limited resources flying to and landing on a non-host
91 tree.^{44,45} At a finer scale, a host tree’s defensive capacity can depend on its canopy position, with reduced
92 biochemical defenses in suppressed, crowded trees.⁴⁶ Coarse-scale measures of forest structure and composition

93 can therefore only partially explain mechanisms affecting bark beetle disturbance. Finer-grain information is
94 also needed that explicitly recognizes tree species, size, and local density, which better capture the ecological
95 processes underlying insect-induced tree mortality.^{28,36,38,39}

96 The vast spatial extent of WPB-induced tree mortality in the 2012 to 2016 California hot drought challenges
97 our ability to simultaneously consider how broad-scale environmental conditions may interact with local
98 forest structure and composition to affect the dynamic between bark beetle selection and colonization of host
99 trees, and host tree susceptibility to attack.^{15,47} Measuring local forest structure generally requires expensive
100 instrumentation^{4,48} or labor-intensive field surveys,^{14,15,49} which constrains survey extent and frequency.
101 Small, unhumanned aerial systems (sUAS) enable relatively fast and cheap remote imaging over hundreds of
102 hectares of forest, which can be used to measure complex forest structure and composition at the individual
103 tree scale with Structure from Motion (SfM) photogrammetry.^{50,51} The ultra-high, centimeter-scale resolution
104 of sUAS-derived measurements as well as the ability to incorporate vegetation reflectance can help overcome
105 challenges in species classification and dead tree detection inherent in other remote sensing methods, such
106 as airborne LiDAR.⁵² Distributing such surveys across an environmental gradient can overcome the data
107 acquisition challenge inherent in investigating phenomena with both a strong local- and a strong broad-scale
108 component.

109 We used sUAS-derived remote sensing images over a network of 32 sites in Sierra Nevada ponderosa pine/mixed-
110 conifer forests spanning 1000 m of elevation and 350 km of latitude¹⁴ covering a total of 9 km², to investigate
111 how broad-scale environmental conditions interacted with local forest structure and composition to shape
112 patterns of tree mortality during the cumulative tree mortality event of 2012 to 2018. We asked:

- 113 1. How does the proportion of the ponderosa pine host trees in a local area and average host tree size
114 affect WPB-induced tree mortality?
- 115 2. How does the density of all trees (hereafter “overall density”) affect WPB-induced tree mortality?
- 116 3. How does the total basal area of all trees (hereafter “overall basal area”) affect WPB-induced tree
117 mortality?
- 118 4. How does environmentally-driven tree moisture stress affect WPB-induced tree mortality?
- 119 5. How do the effects of forest structure, forest composition, and environmental condition interact to
120 influence WPB-induced tree mortality?

121 Here, we show that a greater local proportion of host trees (ponderosa pine) strongly increases the probability
122 of host mortality, with greater host density amplifying this effect. We also show that larger host trees

123 increase the probability of host mortality in accordance with well-known life history of WPB. Critically,
 124 we find a strong interaction between host size and CWD such that larger trees exacerbate host mortality
 125 rates in hot/dry sites. Our results demonstrate a cross-scale interaction in the response of WPB to local
 126 forest structure and composition across an environmental gradient, which helps reconcile differences between
 127 observed ecosystem-wide tree mortality patterns and predictions from models based on coarser-scale forest
 128 structure.

129 Results

130 Tree detection algorithm performance

131 We found that the experimental `lmfx` algorithm⁵³ with parameter values of `dist2d = 1` and `ws = 2.5`
 132 performed the best across 7 measures of forest structure as measured by Pearson’s correlation with ground
 133 data (Table 1).

Table 1: Correlation and differences between the best performing tree detection algorithm (`lmfx` with `dist2d = 1` and `ws = 2.5`) and the ground data. An asterisk next to the correlation or RMSE indicates that this value was within 5% of the value of the best-performing algorithm/parameter set. Ground mean represents the mean value of the forest metric across the 110 field plots that were visible from the sUAS-derived imagery. The median error is calculated as the median of the differences between the air and ground values for the 110 visible plots. Thus, a positive number indicates an overestimate by the sUAS workflow and a negative number indicates an underestimate.

| Forest structure metric | Ground mean | Correlation with ground | RMSE | Median error |
|---|-------------|-------------------------|--------|--------------|
| total tree count | 19 | 0.67* | 8.68* | 2 |
| count of trees > 15 m | 9.9 | 0.43 | 7.38 | 0 |
| distance to 1st neighbor (m) | 2.8 | 0.55* | 1.16* | 0.26 |
| distance to 2nd neighbor (m) | 4.3 | 0.61* | 1.70* | 0.12 |
| height (m); 25 th percentile | 12 | 0.16 | 8.46 | -1.2 |
| height (m); mean | 18 | 0.29 | 7.81* | -2.3 |
| height (m); 75 th percentile | 25 | 0.35 | 10.33* | -4 |

134 Classification accuracy for live/dead and host/non-host

135 The accuracy of live/dead classification on a withheld test dataset was 96.4%. The accuracy of species
 136 classification on a withheld testing dataset was 64.1%. The accuracy of WPB host/non-WPB-host (i.e.,
 137 ponderosa pine versus other tree species) on a withheld testing dataset was 71.8%.

138 **Site summary based on best tree detection algorithm and classification**

139 Across all study sites, we detected, segmented, and classified 452,413 trees in 23,187, 20 x 20m pixels (with
 140 the area of each pixel being approximately equivalent to that of a field plot). Of these trees, we classified
 141 118,879 as dead (26.3% mortality). Estimated site-level tree mortality ranged from 6.8% to 53.6%. See
 142 Supplementary Information for site summaries and comparisons to site-level mortality measured from field
 143 data.

144 **Effect of local structure and regional climate on tree mortality attributed to western pine**
 145 **beetle**

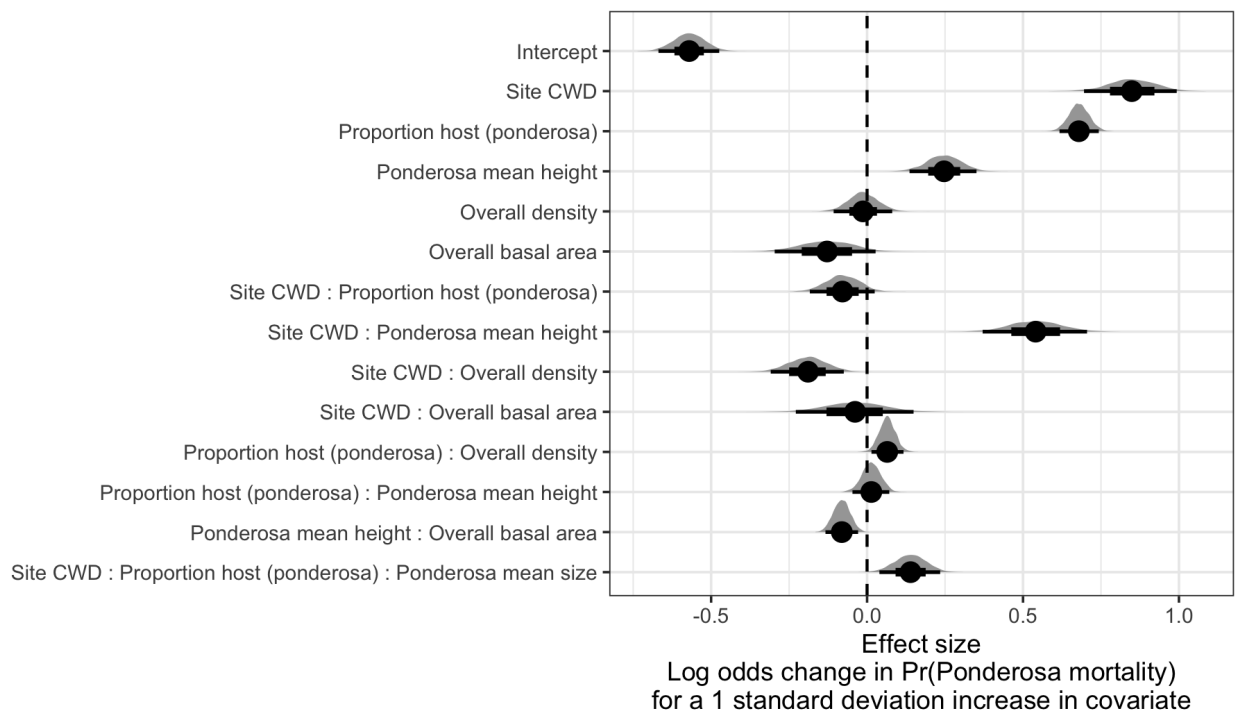


Figure 1: Posterior distributions of effect size from zero-inflated binomial model predicting the probability of ponderosa pine mortality in a 20 x 20-m cell given forest structure characteristics and site-level climatic water deficit (CWD). The gray filled area for each model covariate represents the probability density of the posterior distribution, the point underneath each density curve represents the median of the estimate, the bold interval surrounding the point estimate represents the 66% credible interval, and the thin interval surrounding the point estimate represents the 95% credible interval.

146 Site-level CWD exerted a positive main effect on the probability of ponderosa mortality (effect size: 0.85;
 147 95% CI: [0.70, 0.99]; Figure 1). We found a positive main effect of proportion of host trees per cell (effect size:
 148 0.68; 95% CI: [0.62, 0.74]), with a greater proportion of host trees (i.e., ponderosa pine) in a cell increasing
 149 the probability of ponderosa pine mortality. We detected no effect of overall tree density nor overall basal
 150 area (i.e., including both ponderosa pine and non-host species; tree density effect size: -0.01; 95% CI: [-0.11,

151 0.08]; basal area effect size: -0.13; 95% CI: [-0.29, 0.03]).

152 We found a positive two-way interaction between the overall tree density per cell and the proportion of trees
153 that were hosts, which is equivalent to a positive effect of the density of host trees (effect size: 0.06; 95% CI:
154 [0.01, 0.12]; Figure 1).

155 We found a positive main effect of mean height of ponderosa pine on the probability of ponderosa mortality
156 (effect size: 0.25; 95% CI: [0.14, 0.35]). Coupled with the strong correlation between proportion of dead host
157 trees and basal area killed (See Supplementary Figure 15), these results suggest that WPB attacked larger
158 trees, on average. Further, there was a strong positive interaction between CWD and ponderosa pine mean
159 height, such that larger trees were especially likely to increase the local probability of ponderosa mortality in
160 hotter, drier sites (effect size: 0.54; 95% CI: [0.37, 0.70]; Figure 2).

161 We found no effect of the site-level CWD interactions with the proportion of host trees (effect size: -0.08;
162 95% CI: [-0.18, 0.03]) nor of the interaction between CWD and total basal area (effect size: -0.04; 95% CI:
163 [-0.23, 0.15]; Figure 1).

164 We found a negative effect of the CWD interaction with overall tree density (effect size: -0.19; 95% CI: [-0.31,
165 -0.07]) as well as of the interaction between mean height of host trees and the overall basal area (effect size:
166 -0.08; 95% CI: [-0.13, -0.03]; Figure 1).

167 While we found no interaction between proportion of host trees and mean host tree height, we did find a
168 3-way interaction between these variables with CWD (effect size: 0.14; 95% CI: [0.04, 0.24]; Figure 1).

169 **Discussion**

170 This study uses drone-derived imagery to refine our understanding of the patterns of tree mortality following
171 the 2012 to 2016 California hot drought and its aftermath. By simultaneously measuring the effects of
172 local forest structure and composition across broad-scale environmental gradients, we were able to better
173 characterize the influence of a tree-killing insect, the WPB, compared to using correlates of tree stress alone.

174 **Strong positive main effect of CWD**

175 We found a strong positive effect of site-level CWD on ponderosa pine mortality rate. We did not measure
176 tree water stress at an individual tree level as in other recent work,¹⁵ and instead treated CWD as a general
177 indicator of tree stress following results of coarser-scale studies.¹¹ When measured at a fine scale, even if not
178 at an individual tree level, progressive canopy water loss can be a good indicator of tree water stress and
179 increased vulnerability to mortality from drought or bark beetles.⁵ Though our entire study area experienced

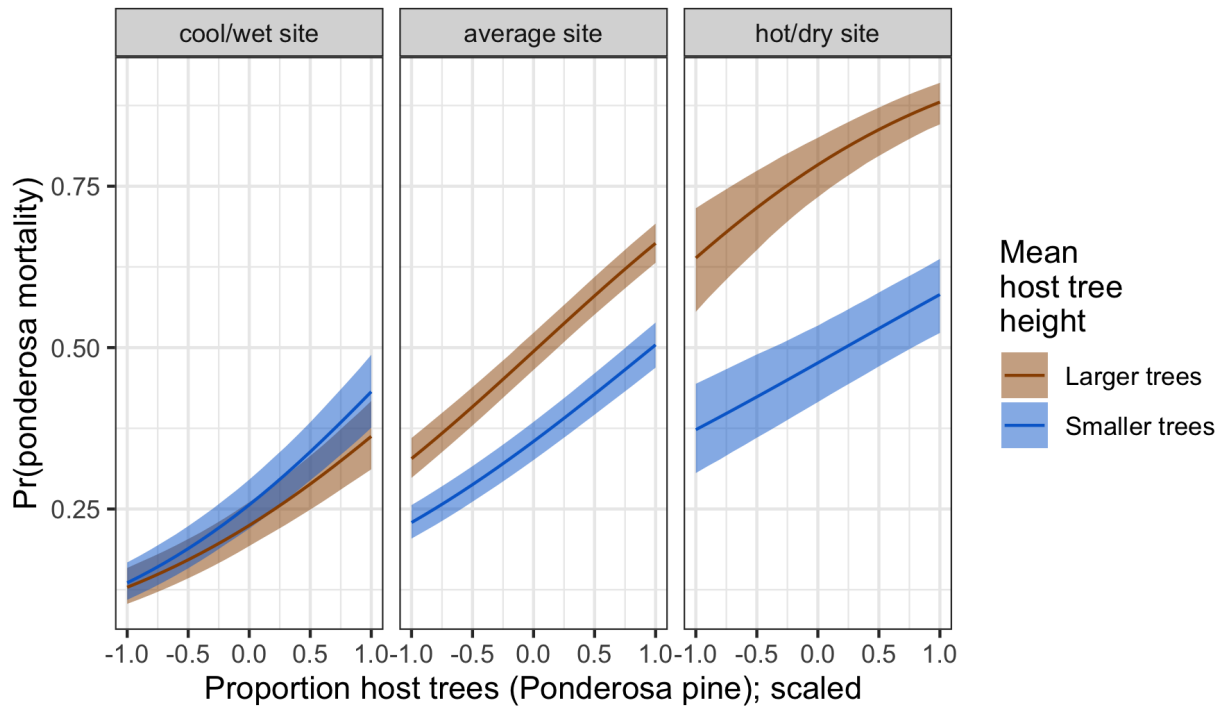


Figure 2: Line version of model results with 95% credible intervals showing primary influence of ponderosa pine structure on the probability of ponderosa pine mortality, and the interaction across climatic water deficit. The ‘larger trees’ line represents the mean height of ponderosa pine 0.7 standard deviations above the mean (approximately 24.1 m), and the ‘smaller trees’ line represents the mean height of ponderosa pine 0.7 standard deviations below the mean (approximately 12.1 m).

180 exceptional hot drought between 2012 and 2015,^{2,3} using a 30-year historic average of CWD as a site-level
181 indicator of tree stress doesn't allow us to disentangle whether water availability was lower in an absolute
182 sense during the drought or whether increasing tree vulnerability to bark beetles was driven by chronic water
183 stress at these historically hotter/drier sites.⁵⁴

184 **Positive effect of host proportion and density**

185 A number of mechanisms associated with the relative abundance of species in a local area might underlie the
186 strong effect of host proportion on the probability of host tree mortality. Frequency-dependent herbivory–
187 whereby mixed-species forests experience less herbivory compared to monocultures (as an extreme example)–
188 is common, especially for oligophagous insect species.⁴⁰ Nonhost volatiles reduce attraction of several species
189 of bark beetles to their aggregation pheromones,⁵⁵ including WPB.⁵⁶ Combinations of nonhost volatiles and
190 an antiaggregation pheromone have been used successfully to reduce levels of tree mortality attributed to
191 WPB in California.^{57,58} The positive relationship between host density and susceptibility to colonization by
192 bark beetles has been so well-documented at the experimental plot level^{43,59,60} that lowering stand densities
193 through selective harvest of hosts is commonly recommended for reducing future levels of tree mortality
194 attributed to bark beetles,⁶¹ including WPB.¹⁸ Greater host density shortens the flight distance required
195 for WPB to disperse to new hosts, which likely facilitates bark beetle spread, however we calibrated our
196 aerial tree detection to ~400 m² areas rather than to individual tree locations, so our data are insufficient to
197 address these relationships. Increased density of ponderosa pine, specifically, may disproportionately increase
198 the competitive environment for host trees (and thus increase their susceptibility to WPB colonization) if
199 intraspecific competition amongst ponderosa pine trees is stronger than interspecific competition as would
200 be predicted with coexistence theory.⁶² Finally, greater host densities increase the frequency that searching
201 WPB land on hosts, rather than nonhosts, thus reducing the amount of energy expended during host finding
202 and selection as well as the time that searching WPB spend exposed to a variety of predators outside the
203 host tree.

204 **No main effect of overall density, but interaction with CWD**

205 We detected no relationship between overall tree density and ponderosa pine mortality, though work from
206 the coincident ground plots showed a negative relationship.¹⁴ 28 also shows greater MPB infestation in
207 lower-density sites in Montana. However, 31 and 14 found that measures of overall tree density explained
208 more variation in tree mortality than measures of host availability, though those conclusions were based on
209 broader-scale analyses³¹ or a different response variable.¹⁴

210 Our greater sample size may have enabled us to more finely parse the role of multi-faceted forest structure
211 and composition, along with CWD and interactions, in driving ponderosa pine mortality rates. Indeed, we
212 did find a negative two-way interaction between site CWD and overall density, suggesting denser stands
213 experienced lower rates of ponderosa mortality in hotter, drier sites, which comports with 9 in results from
214 their unmanipulated gradient of overall density in the same region during the same hot drought. In the
215 absence of active management, forest structure is largely a product of climate and, with increasing importance
216 at finer spatial scales, topographic conditions.⁶³ Denser forest patches in our study may indicate greater local
217 water availability, more favorable conditions for tree growth and survivorship, and increased resistance to
218 beetle-induced tree mortality, especially when denser patches are found in hot, dry sites.^{9,63,64}

219 **Effect of overall basal area**

220 While overall tree density is likely an indicator of favorable microsites in fire-suppressed forests, overall
221 basal area is a better indicator of the local competitive environment especially in water-limited forests.^{63,64}
222 However, we found no main effect of overall basal area on the probability of ponderosa mortality, nor of its
223 interaction with site-level CWD. This contrasts to the results from 11, and from analyses of coincident field
224 plots.¹⁴ While the contrast to 11 might be explained by different scales of analyses (i.e., 3500 x 3500 m pixels
225 vs. 20 x 20 m pixels), the contrast with the coincident ground plots is more puzzling. One explanation is that
226 the drone sampling captured more area beyond the conditionally-sampled field plots (i.e., 10% ponderosa
227 pine basal area mortality was a criterion for plot selection) that reflected a different relationship between
228 local basal area and tree mortality. Perhaps more likely is that our measure of total basal area isn't precise
229 enough to represent the local competitive environment compared to field-derived basal area. For our study,
230 basal area was derived from species-specific and inherently noisy allometric relationships with tree height,
231 which itself was derived from the SfM processing of drone imagery. As remote sensing technology improves
232 to enable finer-scale information extraction (e.g., individual tree measurements), more dialogue between
233 ecologists of all stripes⁶⁵⁻⁶⁷ is needed to fully imagine how to best measure natural phenomena remotely,
234 either by adopting wheels already invented or by innovating something brand new.

235 **Positive main effect of host tree mean size**

236 The positive main effect of host tree mean size on ponderosa mortality rates tracks the conventional wisdom
237 on the dynamics of WPB in the Sierra Nevada, as well as other primary bark beetles.¹⁸ WPB exhibit a
238 preference for trees 50.8 to 76.2 cm DBH,^{68,69} and a positive relationship between host tree size and levels of
239 tree mortality attributed to WPB was reported by 14 in the coincident field plots as well as in other recent
240 studies.^{9,15,70} Larger trees are more nutritious and are therefore ideal targets if local bark beetle density is

241 high enough to successfully initiate mass attack and overwhelm tree defenses, as can occur when many trees
242 are under severe water stress.^{7,13,24} In the recent hot drought, we expected that most trees would be under
243 severe water stress, setting the stage for increasing beetle density, successful mass attacks, and targeting of
244 larger trees. Given that our dead tree height calibration was conservative (accounting for underestimates of
245 drone-derived dead tree heights relative to field-measured trees), it is likely that the positive main effect of tree
246 height that we report represents a lower bounds of this effect. Additionally, 14 found no tree size/mortality
247 relationship for incense cedar or white fir in the coincident field plots. These species represent 22.3% of the
248 total tree mortality observed in their study, yet in our study all dead trees were classified as ponderosa pine
249 (see Methods) which could have further dampened the positive effect of tree size on tree mortality that we
250 identified.

251 **Cross-scale interaction of CWD and host tree size**

252 In hotter, drier sites, a larger average host size increased the probability of host mortality. Notably, a similar
253 pattern was shown by 65 in a study confined to the southern Sierra Nevada (i.e., the hottest, driest portion of
254 the more spatially extensive results we present here) with a strong positive tree height/mortality relationship
255 in areas with the greatest vapor pressure deficit and no tree height/mortality relationship in areas with the
256 lowest vapor pressure deficit. Our work suggests that the WPB was cueing into different aspects of forest
257 structure across an environmental gradient in a spatial context in a parallel manner to the temporal context
258 noted by 65 and 70, who observed that mortality was increasingly driven by larger trees as the hot drought
259 proceeded and became more severe. A temporal signal of bark beetles attacking larger and larger host trees
260 reflects the positive feedback between forest structure and bark beetle population dynamics as the population
261 phase cycles from endemic to epidemic.¹³ This positive feedback leading to eruptive population dynamics
262 is well-documented as a temporal phenomenon, and here we show a similar pattern in a spatial context
263 mediated through site-level CWD.

264 A key difference from the endemic-to-epidemic positive feedback noted by 13 is that none of our study areas
265 were considered to be in an endemic population phase by typical measures of WPB dynamics.^{31,33} WPB
266 dynamics at all sites were considered epidemic, with >5 trees killed per ha (see Supplementary Information).
267 The cross-scale interaction between broad-scale CWD and local-scale host tree size, even amongst populations
268 all in an epidemic phase, highlights the dramatic implications of the positive feedback for landscape-scale
269 tree mortality. The massive tree mortality in hotter/drier Sierra Nevada forests^{4,11} during the 2012 to 2016
270 hot drought likely arose as a synergistic alignment of environmental conditions and local forest structure
271 that allowed WPB to successfully colonize large trees, rapidly increase in population size, and expand. The

272 unexpectedly low mortality in cooler/wetter Sierra Nevada forests compared to model predictions based on
273 coarser-scale forest structure data¹¹ may result from a different WPB response to local forest structure due
274 to a lack of an alignment with favorable climate conditions and a weaker positive feedback.

275 **Limitations and future directions**

276 We have demonstrated that drones can be effective means of collecting forest data at multiple, vastly different
277 spatial scales to investigate a single, multi-scale phenomenon— from meters in between trees, to hundreds of
278 meters of elevation, to hundreds of thousands of meters of latitude. Some limitations remain, but can be
279 overcome with further refinements in the use of this tool for forest ecology. Most of these limitations arise
280 from classification and measurement of standing dead trees, making it imperative to work with field data for
281 calibration and uncertainty reporting.

282 The greatest limitation in our study arising from classification uncertainty is in the assumption that all dead
283 trees were ponderosa pine, which we estimate from coincident field plots is true approximately 73.4% of the
284 time. Because the forest structure factors influencing the likelihood of individual tree mortality during the hot
285 drought depended on tree species,¹⁵ we cannot rule out that some of the ponderosa pine mortality relationships
286 to forest structure that we observed may be partially explained by those relationships in other species that
287 were misclassified as ponderosa pine using our methods. However, the overall community composition across
288 our study area was similar¹⁴ and we are able to reproduce similar forest structure/mortality patterns in
289 drone-derived data when restricting the scope of analysis to only trees detected in the footprints of the
290 coincident field plots (see Supplementary Information). Thus, we remain confident that the patterns we
291 observed were driven primarily by the dynamic between WPB and ponderosa pine. While spectral information
292 of foliage could help classify living trees to species, the species of standing dead trees were not spectrally
293 distinct. This challenge of classifying standing dead trees to species implies that a conifer forest systems with
294 less bark beetle and tree host diversity, such as mountain pine beetle outbreaks in relative monocultures of
295 naturally-occurring lodgepole pine forests in the Intermountain West, should be particularly amenable to the
296 methods presented here even with minimal further refinement because dead trees will almost certainly belong
297 to a single species and have succumbed to colonization by a single bark beetle species. For similar reasons,
298 these methods would also work particularly well if imagery were also captured prior to the mortality event.

299 Some uncertainty surrounded our ability to detect trees using the geometry of the dense point clouds derived
300 with SfM. The horizontal accuracy (i.e., longitude/latitude position) of the tree detection was better than the
301 vertical accuracy (i.e., height), which may result from a more significant error contribution by the field-based
302 calculations of tree height compared to tree position relative to plot center (Table 1). Height measurements

303 were particularly challenging for standing dead trees, because SfM can fail to produce any points representing
304 narrow, needleless treetops in the resulting dense point cloud. Our conservative calibration of drone-measured
305 tree heights to field-measured heights strengthened the main effect of CWD on host mortality in our model
306 and reversed the effect of host tree height (see Supplementary Information). We report that larger host trees
307 increase the probability of host tree mortality, while models using uncalibrated tree heights show that larger
308 trees decrease host mortality rates (see Supplementary Information). While our live/dead classification was
309 fairly accurate (96.4% on a withheld dataset), our species classifier would likely benefit from better crown
310 segmentation because the pixel-level reflectance values within each crown are averaged to characterize the
311 “spectral signature” of each tree. With better delineation of each tree crown, the mean value of pixels within
312 each tree crown will likely be more representative of that tree’s spectral signature.

313 Better tree detection, crown segmentation, and dead tree height measurement would likely improve with
314 better SfM point clouds which can be enhanced with greater overlap between images⁷¹ or with oblique (i.e.,
315 off-nadir) imagery.⁷² 71 found that 95% overlap was preferable for generating dense point clouds in forested
316 areas, and 72 reduced dense point cloud errors using imagery taken at 30 degrees off-nadir. We only achieved
317 91.6% overlap with the X3 RGB camera and 83.9% overlap with the multispectral camera, and all imagery
318 was nadir-facing. We anticipate that computer vision and deep learning will also prove helpful in overcoming
319 some of these detection and classification challenges.⁷³

320 Finally, we note our study is constrained by the uncertainty in measuring basal area from SfM processing of
321 drone-derived imagery. This uncertainty makes it challenging to represent typical field-based measures of
322 local competitive environment (e.g., total plot basal area) or ecosystem impact (e.g., proportion of dead basal
323 area in a plot) in a statistical analysis. Instead, we opted to use the probability of ponderosa mortality as
324 our key response variable, which is well-suited to understanding the dynamics between WPB colonization
325 behavior and host tree susceptibility.

326 **Conclusions**

327 Climate change adaptation strategies emphasize management action that considers whole-ecosystem responses
328 to inevitable change,⁷⁴ which requires a macroecological understanding of how phenomena at multiple
329 scales can interact. Tree vulnerability to environmental stressors presents only a partial explanation for
330 tree mortality patterns during hot droughts, especially when bark beetles are present. We’ve shown that
331 drones can be a valuable tool for investigating multi-scalar phenomena, such as how local forest structure
332 combines with environmental conditions to shape forest insect disturbance. Understanding the conditions
333 that drive dry western U.S. forest responses to disturbances such as bark beetle outbreaks will be vital for

334 predicting outcomes from increasing disturbance frequency and intensity exacerbated by climate change.⁷⁵
335 Our study suggests that outcomes will depend on interactions between local forest structure and broad-scale
336 environmental gradients, with the potential for cross-scale interactions to enhance our understanding of forest
337 insect dynamics.

338 **Methods**

339 **Study system**

340 We designed the aerial survey to coincide with 160 vegetation/forest insect monitoring plots at 32 sites
341 established between 2016 and 2017 by 14 (Figure 3). The study sites were chosen to reflect typical west-side
342 Sierra Nevada yellow pine/mixed-conifer forests and were dominated by ponderosa pine.¹⁴ Sites were placed
343 in WPB-attacked, yellow pine/mixed-conifer forests across the Eldorado, Stanislaus, Sierra and Sequoia
344 National Forests and were stratified by elevation (914-1219 m, 1219-1524 m, 1524-1829 m above sea level). In
345 the Sequoia National Forest, the southernmost National Forest in our study, sites were stratified with the
346 lowest elevation band of 1219-1524 m and extended to an upper elevation band of 1829-2134 m to capture a
347 more similar forest community composition as at the more northern National Forests. The sites have variable
348 forest structure and plot locations were selected in areas with >35% ponderosa pine basal area and >10%
349 ponderosa pine mortality. At each site, five 0.041-ha circular plots were installed along transects with 80
350 to 200m between plots. In the field, 14 mapped all stem locations relative to the center of each plot using
351 azimuth/distance measurements. Tree identity to species, tree height, and diameter at breast height (DBH)
352 were recorded if DBH was greater than 6.35cm. Year of mortality was estimated based on needle color and
353 retention if it occurred prior to plot establishment, and was directly observed thereafter during annual site
354 visits. A small section of bark (approximately 625 cm²) on both north and south aspects was removed from
355 dead trees to determine if bark beetle galleries were present. The shape, distribution, and orientation of
356 galleries are commonly used to distinguish among bark beetle species.¹⁸ In some cases, deceased bark beetles
357 were present beneath the bark to supplement identifications based on gallery formation. During the spring
358 and early summer of 2018, all field plots were revisited to assess whether dead trees had fallen.¹⁴

359 In the typical life cycle of WPBs, females initiate host colonization by tunneling through the outer bark and
360 into the phloem and outer xylem where they rupture resin canals. As a result, oleoresin exudes and collects on
361 the bark surface, as is commonly observed with other bark beetle species. During the early stages of attack,
362 females release an aggregation pheromone component which, in combination with host monoterpenes released
363 from pitch tubes, is attractive to conspecifics.⁷⁶ An antiaggregation pheromone component is produced during
364 latter stages of host colonization by several pathways, and is thought to reduce intraspecific competition

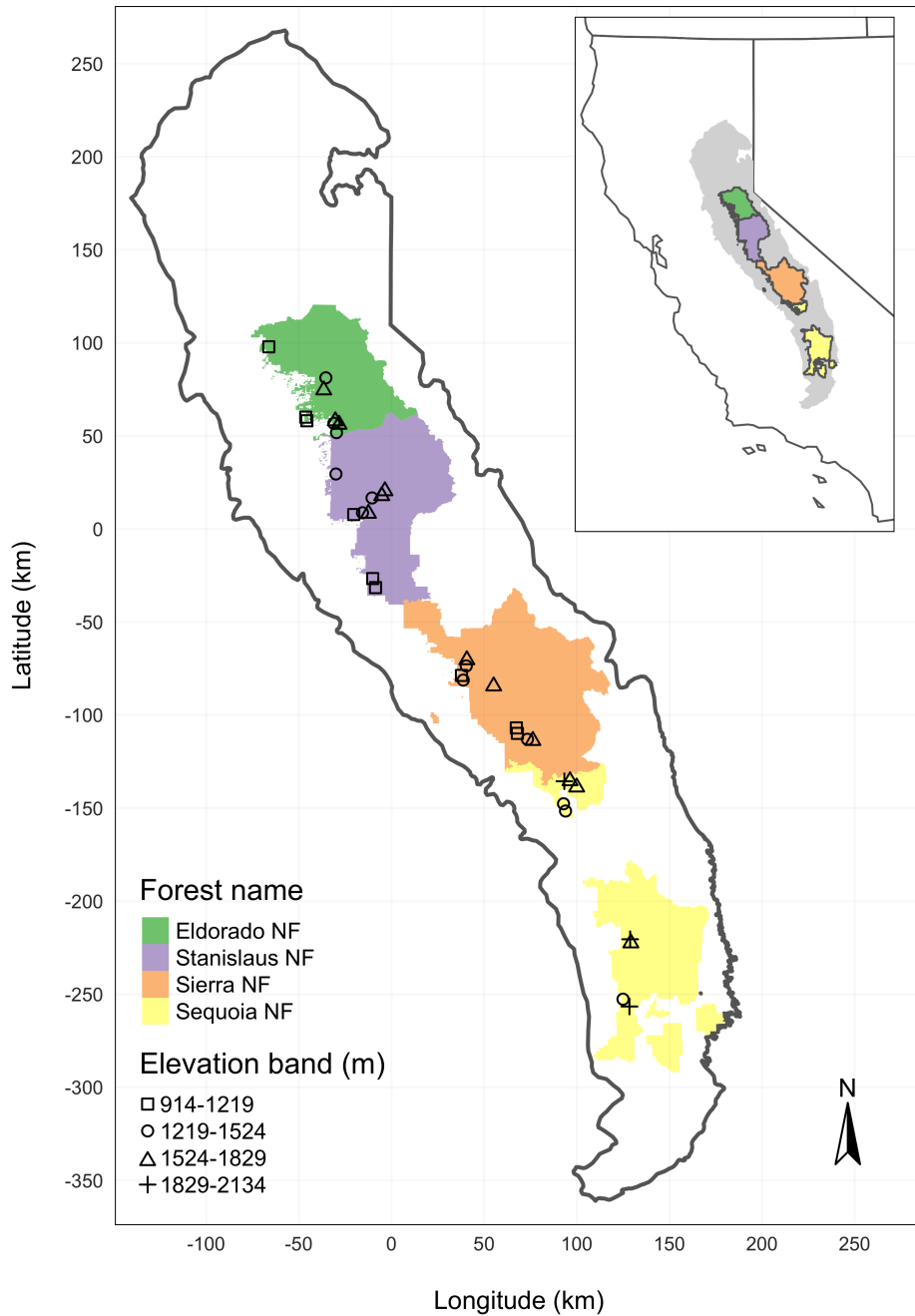


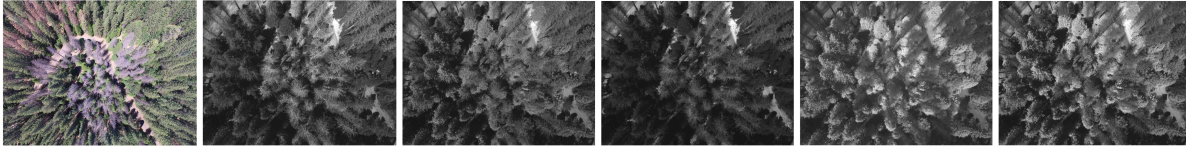
Figure 3: The network of field plots spanned a 350-km latitudinal gradient from the Eldorado National Forest in the north to the Sequoia National Forest in the south. Plots were stratified by three elevation bands in each forest, with the plots in the Sequoia National Forest (the southern-most National Forest) occupying elevation bands 305 m above the three bands in the other National Forests in order to capture a similar community composition.

365 by altering adult behavior to minimize overcrowding of developing brood within the host.⁷⁷ Volatiles from
366 several nonhosts sympatric with ponderosa pine have been demonstrated to inhibit attraction of WPB to
367 its aggregation pheromones.^{56,78} In California, WPB generally has 2-3 generations in a single year and can
368 often outcompete other primary bark beetles such as the mountain pine beetle in ponderosa pines, especially
369 in larger trees.³³ WPB population growth rates can, however, be reduced by competition with other beetle
370 species cohabitating in the same host tree, as well as by predation during dispersal to seek a host.³³

371 **Aerial data collection and processing**

372 Nadir-facing imagery was captured using a gimbal-stabilized DJI Zenmuse X3 broad-band red/green/blue
373 (RGB) camera⁷⁹ and a fixed-mounted Micasense Rededge3 multispectral camera with five narrow bands⁸⁰ on
374 a DJI Matrice 100 aircraft.⁸¹ Imagery was captured from both cameras along preprogrammed aerial transects
375 over ~40 ha surrounding each of the 32 sites (each of these containing five field plots) and was processed in a
376 series of steps to yield local forest structure and composition data suitable for our statistical analyses. All
377 images were captured in 2018 during a 3-month period between early April and early July, and thus our work
378 represents a postmortem investigation into the drivers of cumulative tree mortality. Following the call by 82,
379 we establish “data product levels” to reflect the image processing pipeline from raw imagery (Level 0) to
380 calibrated, fine-scale forest structure and composition information on regular grids (Level 4), with each new
381 data level derived from levels below it. Here, we outline the steps in the processing and calibration pipeline
382 visualized in Figure 4, and include additional details in the Supplementary Information.

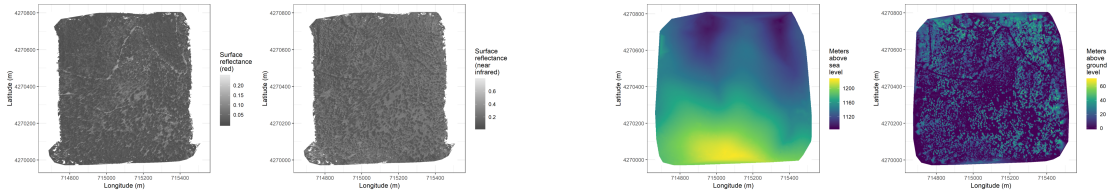
Level 0: raw data from sensors



Level 1: basic outputs from photogrammetric processing



Level 2: corrected outputs from photogrammetric processing

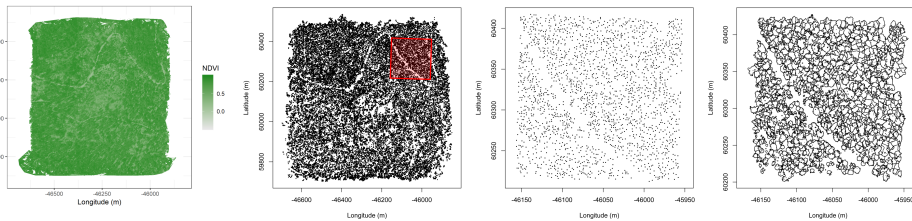


radiometric (e.g., normalize for atmosphere)

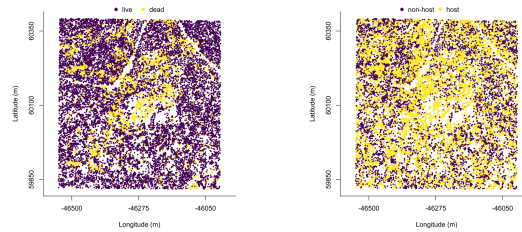
geometric (e.g., normalize for terrain)

Level 3: domain-specific information extraction

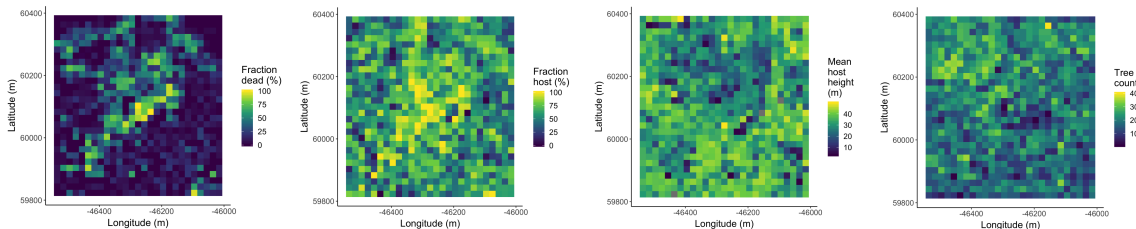
L3a
spectral
OR
geometric



L3b
spectral
AND
geometric



Level 4: aggregations to regular grids



384 Figure 4. Schematic of the data processing workflow for a single site with each new data product level derived
385 from data at lower levels. Level 0 represents raw data from the sensors. From left to right: RGB photo from
386 DJI Zenmuse X3, output images from Micasense Rededge3 (blue, green, red, near infrared, red edge). Level 1
387 represents basic outputs from the SfM workflow. From left to right: dense point cloud, RGB orthophoto,
388 digital surface model (DSM; ground elevation plus vegetation height). Level 2 represents radiometrically
389 or geometrically corrected Level 1 products. From left to right: radiometrically-corrected “red” surface
390 reflectance map, radiometrically-corrected “near infrared” surface reflectance map, digital terrain model
391 (DTM) derived by a geometric correction of the dense point cloud, canopy height model (CHM; DSM - DTM).
392 Level 3 represents domain-specific information extraction from Level 2 products and is divided into two
393 sub-levels. Level 3a products are derived using only spectral or only geometric data. From left to right: map
394 of Normalized Difference Vegetation Index,⁸³ map of detected trees derived from the CHM, detected trees
395 within red polygon, polygons representing segmented tree crowns within red polygon. Level 3b products are
396 derived using both spectral and geometric data. From left to right: trees classified as alive or dead based
397 on spectral reflectance within each segmented tree crown, trees classified as WPB host/non-host. Level 4
398 represents aggregations of Level 3 products to regular grids that better reflects the grain size of the validation
399 (e.g., to match area of validation field plots) or which provides neighborhood- rather than individual-scale
400 information (e.g., stand-level proportion of host trees). From left to right: grid representing fraction of dead
401 trees per cell, grid representing fraction of hosts per cell, grid representing mean host height per cell, tree
402 density per cell. All cells measure 20 x 20 m.

403 **Level 0: Raw data from sensors**

404 Raw data comprised approximately 1900 images per camera lens (one broad-band RGB lens and five narrow-
405 band multispectral lenses) for each of the 32 sites (Figure 4; Level 0). Prior to the aerial survey, two strips of
406 bright orange drop cloth (~100 x 15 cm) were positioned as an “X” over the permanent monuments marking
407 the center of the 5 field plots from 14 (see Supplementary Information).

408 We preprogrammed north-south aerial transects using Map Pilot for DJI on iOS flight software⁸⁴ at an
409 altitude of 120 m above ground level (with “ground” defined using a 1-arc-second digital elevation model⁸⁵).
410 The resulting ground sampling distance was approximately 5 cm/px for the Zenmuse X3 RGB camera and
411 approximately 8 cm/px for the Rededge3 multispectral camera. We used 91.6% image overlap (both forward
412 and side) at the ground for the Zenmuse X3 RGB camera and 83.9% overlap (forward and side) for the
413 Rededge3 multispectral camera.

414 **Level 1: Basic outputs from photogrammetric processing**

415 We used SfM photogrammetry implemented in Pix4Dmapper Cloud (www.pix4d.com) to generate dense point
416 clouds (Figure 4; Level 1, left), orthophotos (Figure 4; Level 1, center), and digital surface models (Figure 4;
417 Level 1, right) for each field site.⁷¹ For 29 sites, we processed the Rededge3 multispectral imagery alone to
418 generate these products. For three sites, we processed the RGB and the multispectral imagery together to
419 enhance the point density of the dense point cloud. All SfM projects resulted in a single processing “block,”
420 indicating that all images in the project were optimized and processed together. The dense point cloud
421 represents x, y, and z coordinates as well as the color of millions of points per site. The orthophoto represents
422 a radiometrically uncalibrated, top-down view of the survey site that preserves the relative x-y positions of
423 objects in the scene. The digital surface model is a rasterized version of the dense point cloud that shows
424 the altitude above sea level for each pixel in the scene at the ground sampling distance of the camera that
425 generated the Level 0 data.

426 **Level 2: Corrected outputs from photogrammetric processing**

427 **Radiometric corrections** A radiometrically-corrected reflectance map (Figure 4; Level 2, left two figures;
428 i.e., a corrected version of the Level 1 orthophoto) was generated using the Pix4D software by incorporating
429 incoming light conditions for each narrow band of the Rededge3 camera (captured simultaneously with the
430 Rededge3 camera using an integrated downwelling light sensor) as well as a pre-flight image of a calibration
431 panel of known reflectance (see Supplementary Information for camera and calibration panel details).

432 **Geometric corrections** We implemented a geometric correction to the Level 1 dense point cloud and
433 digital surface model by normalizing these data for the terrain underneath the vegetation. We generated the
434 digital terrain model representing the ground underneath the vegetation at 1-m resolution (Figure 4; Level
435 2, third image) by classifying each survey area’s dense point cloud into “ground” and “non-ground” points
436 using a cloth simulation filter algorithm⁸⁶ implemented in the `lidR`⁵³ package and rasterizing the ground
437 points using the `raster` package.⁸⁷ We generated a canopy height model (Figure 4; Level 2, fourth image) by
438 subtracting the digital terrain model from the digital surface model.

439 **Level 3: Domain-specific information extraction**

440 **Level 3a: Data derived from spectral or geometric Level 2 product** Using just the spectral
441 information from the radiometrically-corrected reflectance maps, we calculated several vegetation indices
442 including the normalized difference vegetation index [NDVI; 83; Figure 4; Level 3a, first image], the normalized
443 difference red edge,⁸⁸ the red-green index,⁸⁹ the red edge chlorophyll index,⁹⁰ and the green chlorophyll

Table 2: Algorithm name, number of parameter sets tested for each algorithm, and references.

| Algorithm | Parameter sets tested | Reference(s) |
|-------------|-----------------------|--------------|
| li2012 | 131 | 91; 92; 93 |
| lmfx | 30 | 94 |
| localMaxima | 6 | 53 |
| multichm | 1 | 95 |
| ptrees | 3 | 96 |
| vwf | 3 | 97 |
| watershed | 3 | 98 |

445 Using just the geometric information from the canopy height model or terrain-normalized dense point cloud,
446 we generated maps of detected trees (Figure 4; Level 3a, second and third images) by testing a total of 7
447 automatic tree detection algorithms and a total of 177 parameter sets (Table 2). We used the field plot data
448 to assess each tree detection algorithm/parameter set by converting the distance-from-center and azimuth
449 measurements of the trees in the field plots to x-y positions relative to the field plot centers distinguishable in
450 the Level 2 reflectance maps as the orange fabric X’s that we laid out prior to each flight. In the reflectance
451 maps, we located 110 out of 160 field plot centers while some plot centers were obscured due to dense
452 interlocking tree crowns or because a plot center was located directly under a single tree crown. For each of
453 the 110 field plots with identifiable plot centers– the “validation field plots”, we calculated 7 forest structure
454 metrics using the ground data collected by 14: total number of trees, number of trees greater than 15 m
455 in height, mean height of trees, 25th percentile tree height, 75th percentile tree height, mean distance to
456 nearest tree neighbor, and mean distance to second nearest neighbor. For each tree detection algorithm and
457 parameter set described above, we calculated the same set of 7 structure metrics within the footprint of the
458 validation field plots. We calculated the Pearson’s correlation and root mean square error (RMSE) between
459 the ground data and the aerial data for each of the 7 structure metrics for each of the 177 automatic tree
460 detection algorithms/parameter sets. For each algorithm and parameter set, we calculated its performance
461 relative to other algorithms as whether its Pearson’s correlation was within 5% of the highest Pearson’s
462 correlation as well as whether its RMSE was within 5% of the lowest RMSE. We summed the number of
463 forest structure metrics for which it reached these 5% thresholds for each algorithm/parameter set. For
464 automatically detecting trees across the whole study, we selected the algorithm/parameter set that performed

465 well across the most forest metrics (see Results).

466 We delineated individual tree crowns (Figure 4; Level 3a, fourth image) with a marker controlled watershed
467 segmentation algorithm⁹⁹ implemented in the `ForestTools` package⁹⁷ using the detected treetops as markers.
468 If the automatic segmentation algorithm failed to generate a crown segment for a detected tree (e.g., often
469 snags with a very small crown footprint), a circular crown was generated with a radius of 0.5 m. If the
470 segmentation generated multiple polygons for a single detected tree, only the polygon containing the detected
471 tree was retained. Because image overlap decreases near the edges of the overall flight path and reduces the
472 quality of the SfM processing in those areas, we excluded segmented crowns within 35 m of the edge of the
473 survey area. Given the narrower field of view of the Rededge3 multispectral camera versus the X3 RGB
474 camera whose optical parameters were used to define the ~40 ha survey area around each site, as well as the
475 35 m additional buffering, the survey area at each site was ~30 ha (see Supplementary Information).

476 **Level 3b: Data derived from spectral and geometric information** We overlaid the segmented
477 crowns on the reflectance maps from 20 sites spanning the latitudinal and elevation gradient in the study.
478 Using QGIS (<https://qgis.org/en/site/>), we hand classified 564 trees as live/dead and as one of 5 dominant
479 species in the study area (ponderosa pine, *Pinus lambertiana*, *Abies concolor*, *Calocedrus decurrens*, or *Quercus*
480 *kelloggi*) using the mapped ground data as a guide. Each tree was further classified as “host” for ponderosa
481 pine or “non-host” for all other species.¹⁸ We extracted all the pixel values within each segmented crown
482 polygon from the five, Level 2 orthorectified reflectance maps (one per narrow band on the Rededge3 camera)
483 as well as from the five, Level 3a vegetation index maps using the `velox` package.¹⁰⁰ For each crown polygon,
484 we calculated the mean value of the extracted Level 2 and Level 3a pixels and used them as ten independent
485 variables in a five-fold cross validated boosted logistic regression model to predict whether the hand classified
486 trees were alive or dead. For just the living trees, we similarly used all 10 mean reflectance values per crown
487 polygon to predict tree species using a five-fold cross validated regularized discriminant analysis. The boosted
488 logistic regression and regularized discriminant analysis were implemented using the `caret` package in R.¹⁰¹
489 We used these models to classify all tree crowns in the data set as alive or dead (Figure 4; Level 3b, first
490 image) as well as the species of living trees (Figure 4; Level 3b, second image).

491 Because the tops of dead, needle-less trees are narrow, they may not be well-represented in the point
492 clouds produced using SfM photogrammetry, which biases their height estimates downward. Further, field
493 measurements can overestimate the heights of live trees relative to aerial survey methods.¹⁰² To correct these
494 measurement biases, we calibrated aerial tree height measurements to ground-based height measurements.
495 Specifically, we identified the crowns of 451 field-measured trees in the drone-derived tree data, modeled the

496 relationship between field- and drone-measured tree heights for both live and dead trees, and used the models
497 to adjust the drone-measured tree heights (See Supplementary Methods). We applied a conservative height
498 correction to live and dead trees based on trees measured by the drone to be greater than 20 m in height
499 that increased dead tree height by an average of 2.8 m and reduced the heights of live trees by an average of
500 0.9 m (See Supplementary Methods). Finally, we estimated the basal area of each tree from their corrected
501 drone-measured height using species-specific simple linear regressions of the relationship between height and
502 DBH as measured in the coincident field plots from 14.

503 **Level 4: Aggregations to regular grids**

504 We rasterized the forest structure and composition data at a spatial resolution similar to that of the field
505 plots to better match the grain size at which we validated the automatic tree detection algorithms. In each
506 raster cell, we calculated: number of dead trees, number of ponderosa pine trees, total number of trees, and
507 mean height of ponderosa pine trees. The values of these variables in each grid cell and derivatives from
508 them were used for visualization and modeling. Here, we show the fraction of dead trees per cell (Figure 4;
509 Level 4, first image), the fraction of host trees per cell (Figure 4; Level 4, second image), the mean height of
510 ponderosa pine trees in each cell (Figure 4; Level 4, third image), and the total count of trees per cell (Figure
511 4; Level 4, fourth image).

512 **Note on assumptions about dead trees**

513 For the purposes of this study, we assumed that all dead trees were ponderosa pine and thus hosts colonized
514 by WPB. This is a reasonably good assumption for our study area; for example, 14 found that 73.4% of dead
515 trees in their coincident field plots were ponderosa pine. Mortality was concentrated in the larger-diameter
516 classes and attributed primarily to WPB.¹⁴ The species contributing to the next highest proportion of dead
517 trees was incense cedar which represented 18.72% of the dead trees in the field plots. While the detected
518 mortality is most likely to be ponderosa pine killed by WPB, it is critical to interpret our results with these
519 limitations in mind.

520 **Environmental data**

521 We used CWD¹⁰³ from the 1981-2010 mean value of the basin characterization model¹⁰⁴ as an integrated
522 measure of historic temperature and moisture conditions for each of the 32 sites. Higher values of CWD
523 correspond to historically hotter, drier conditions and lower values correspond to historically cooler, wetter
524 conditions. CWD has been shown to correlate well with broad patterns of tree mortality in the Sierra
525 Nevada¹¹ as well as bark beetle-induced tree mortality.¹⁰⁵ The forests along the entire CWD gradient used in

526 this study experienced exceptional hot drought between 2012 to 2016 with a severity of at least a 1,200-year
527 event, and perhaps more severe than a 10,000-year event.^{2,3} We converted the CWD value for each site into a
528 z-score representing that site’s deviation from the mean CWD across the climatic range of Sierra Nevada
529 ponderosa pine as determined from 179 herbarium records described in 106. Thus, a CWD z-score of 1 would
530 indicate that the CWD at that site is one standard deviation hotter/drier than the mean CWD across all
531 geolocated herbarium records for ponderosa pine in the Sierra Nevada.

532 **Statistical model**

533 We used a generalized linear model with a zero-inflated binomial response and a logit link to predict the
534 probability of ponderosa pine mortality within each 20 x 20-m cell using the total number of ponderosa
535 pine trees in each cell as the number of trials, and the number of dead trees in each cell as the number of
536 “successes”. As covariates, we used the proportion of trees that are WPB hosts (i.e., ponderosa pine) in each
537 cell, the mean height of ponderosa pine trees in each cell, the count of trees of all species (overall density) in
538 each cell, and the site-level CWD using Eq. 1. Note that the two-way interaction between the overall density
539 and the proportion of trees that are hosts is directly proportional to the number of ponderosa pine trees in
540 the cell. We centered and scaled all predictor values, and used weakly-regularizing default priors from the
541 `brms` package.¹⁰⁷ To measure and account for spatial autocorrelation underlying ponderosa pine mortality,
542 we subsampled the data at each site to a random selection of 200, 20 x 20-m cells representing approximately
543 27.5% of the surveyed area. Additionally with these subsampled data, we included a separate exact Gaussian
544 process term per site of the noncentered/nonscaled interaction between the x- and y-position of each cell
545 using the `gp()` function in the `brms` package.¹⁰⁷ The Gaussian process estimates the spatial covariance in the
546 response variable (log-odds of ponderosa pine mortality) jointly with the effects of the other covariates.

$$y_{i,j} \sim \begin{cases} 0, & p \\ \text{Binom}(n_i, \pi_i), & 1 - p \end{cases}$$

$$\begin{aligned} \text{logit}(\pi_i) = & \beta_0 + \\ & \beta_1 X_{cwd,j} + \beta_2 X_{propHost,i} + \beta_3 X_{PipoHeight,i} + \\ & \beta_4 X_{overallDensity,i} + \beta_5 X_{overallBA,i} + \\ & \beta_6 X_{cwd,j} X_{PipoHeight,i} + \beta_7 X_{cwd,j} X_{propHost,i} + \\ & \beta_8 X_{cwd,j} X_{overallDensity,i} + \beta_9 X_{cwd,j} X_{overallBA,i} + \\ & \beta_{10} X_{propHost,i} X_{PipoHeight,i} + \beta_{11} X_{propHost,i} X_{overallDensity,i} + \\ & \beta_{12} X_{PipoHeight,i} X_{overallBA,i} + \\ & \beta_{13} X_{cwd,j} X_{propHost,i} X_{PipoHeight,i} + \\ & \mathcal{GP}_j(x_i, y_i) \end{aligned} \tag{1}$$

547 Where y_i is the number of dead trees in cell i , n_i is the sum of the dead trees (assumed to be ponderosa pine)
548 and live ponderosa pine trees in cell i , π_i is the probability of ponderosa pine tree mortality in cell i , p is the
549 probability of there being zero dead trees in a cell arising as a result of an independent, unmodeled process,
550 $X_{cwd,j}$ is the z-score of CWD for site j , $X_{propHost,i}$ is the scaled proportion of trees that are ponderosa pine
551 in cell i , $X_{PipoHeight,i}$ is the scaled mean height of ponderosa pine trees in cell i , $X_{overallDensity,i}$ is the scaled
552 density of all trees in cell i , $X_{overallBA,i}$ is the scaled basal area of all trees in cell i , x_i and y_i are the x- and
553 y- coordinates of the centroid of the cell in an EPSG3310 coordinate reference system, and \mathcal{GP}_j represents
554 the exact Gaussian process describing the spatial covariance between cells at site j .

555 We fit this model using the `brms` package¹⁰⁷ which implements the No U-Turn Sampler extension to the
556 Hamiltonian Monte Carlo algorithm¹⁰⁸ in the Stan programming language.¹⁰⁹ We used 4 chains with 5000
557 iterations each (2000 warmup, 3000 samples), and confirmed chain convergence by ensuring all `Rhat` values
558 were less than 1.1¹¹⁰ and that the bulk and tail effective sample sizes (ESS) for each estimated parameter
559 were greater than 100 times the number of chains (i.e., greater than 400 in our case). We used posterior
560 predictive checks to visually confirm model performance by overlaying the density curves of the predicted
561 number of dead trees per cell over the observed number.¹¹¹ For the posterior predictive checks, we used 50
562 random samples from the model fit to generate 50 density curves and ensured curves were centered on the
563 observed distribution, paying special attention to model performance at capturing counts of zero.

564 **Data availability**

565 All field and drone data processed for this study are available via the Open Science Framework at <https://doi.org/10.17605/OSF.IO/3CWF9>.¹¹² The administrative boundaries file for the USDA Forest Service
566 (S_USA.AdministrativeForest.shp) can be found at [https://data.fs.usda.gov/geodata/edw/datasets.ph](https://data.fs.usda.gov/geodata/edw/datasets.php?dsetCategory=boundaries)
567 [p?dsetCategory=boundaries](https://data.fs.usda.gov/geodata/edw/datasets.php?dsetCategory=boundaries). The 2014 version of the 1981-2010 thirty-year historic average climatic water
568 deficit data (cwd1981_2010_ave_HST_1550861123.tif) can be found on the California Climate Commons
569 at <http://climate.calcommons.org/dataset/2014-CA-BCM>. The dataset representing ponderosa pine
570 geolocations derived from herbaria records (California_Species_clean_All_epsg_3310.csv) can be found
571 at <https://doi.org/10.6078/D16K5W>.¹¹³ The vector file representing Jepson geographic subdivisions of
572 California and used to define the Sierra Nevada region can be requested at <https://ucjeps.berkeley.edu/eflora>
573 [/geography.html](https://ucjeps.berkeley.edu/eflora/geography.html).
574

575 **Code availability**

576 Statistical analyses were performed using the `brms` packages. With the exception of the SfM software
577 (Pix4Dmapper Cloud) and the GIS software QGIS, all data carpentry and analyses were performed using
578 R.¹¹⁴ All code used to generate the results from this study are available via GitHub at [https://github](https://github.com/mikoontz/local-structure-wpb-severity)
579 [ub.com/mikoontz/local-structure-wpb-severity](https://github.com/mikoontz/local-structure-wpb-severity) and is mirrored on the Open Science Framework at
580 <https://doi.org/10.17605/OSF.IO/WPK5Z>.¹¹⁵

581 **Acknowledgements**

582 We gratefully acknowledge funding from the USDA Forest Service Western Wildlands Environmental Threat
583 Assessment Center (WWETAC) and the Pacific Southwest Research Station Climate Change Competitive
584 Grant Program. We thank Connie Millar for comments and guidance during the development of this project,
585 Victoria Scholl for helpful discussions regarding remotely-sensed data product levels, and Derek Young for
586 helpful discussions while revising this manuscript. We also thank Meagan Oldfather for her role as visual
587 observer during drone flights. We gratefully acknowledge Pix4D, which provided free cloud infrastructure
588 for much of the Structure from Motion photogrammetry processing. Finally, we thank the Open Science
589 Framework for facilitating the public access to our complete dataset.

590 **Author contributions**

591 Author contributions are defined using the Contributor Roles Taxonomy (CRediT; <https://casrai.org/credit/>).
592 Conceptualization: MJK, AML, CJF, MPN, LAM; Data curation: MJK; Formal analysis: MJK; Funding

593 acquisition: MJK, MPN, CJF, AML; Investigation: MJK, LAM, CJF; Methodology: MJK, AML; Project
594 administration: MJK; Resources: MJK, MPN, AML; Software: MJK; Supervision: MJK, MPN, AML;
595 Validation: MJK; Visualization: MJK; Writing – original draft: MJK; Writing – review and editing: MJK,
596 AML, CJF, MPN, LAM

597 **Competing interests**

598 The authors declare no competing interests.

References

- 599 1. USDAFS. Press Release: Survey finds 18 million trees died in California in 2018. [https://www.fs.usda.gov](https://www.fs.usda.gov/Internet/FSE_DOCUMENTS/FSEPRD609321.pdf)
600 v/Internet/FSE_DOCUMENTS/FSEPRD609321.pdf (2019).
- 602 2. Griffin, D. & Anchukaitis, K. J. How unusual is the 2012-2014 California drought? *Geophysical Research*
603 *Letters* **41**, 9017–9023 (2014).
- 604 3. Robeson, S. M. Revisiting the recent California drought as an extreme value. *Geophysical Research Letters*
605 **42**, 6771–6779 (2015).
- 606 4. Asner, G. P. *et al.* Progressive forest canopy water loss during the 2012-2015 California drought. *Proceedings*
607 *of the National Academy of Sciences* **113**, E249–E255 (2016).
- 608 5. Brodrick, P. G. & Asner, G. P. Remotely sensed predictors of conifer tree mortality during severe drought.
609 *Environ. Res. Lett.* **12**, 115013 (2017).
- 610 6. Fettig, C. J. Chapter 2: Forest health and bark beetles. in *Managing Sierra Nevada Forests. PSW-GTR-237*
611 (USDA Forest Service, 2012).
- 612 7. Kolb, T. E. *et al.* Observed and anticipated impacts of drought on forest insects and diseases in the United
613 States. *Forest Ecology and Management* **380**, 321–334 (2016).
- 614 8. Waring, R. H. & Pitman, G. B. Modifying lodgepole pine stands to change susceptibility to mountain pine
615 beetle attack. *Ecology* **66**, 889–897 (1985).
- 616 9. Restaino, C. *et al.* Forest structure and climate mediate drought-induced tree mortality in forests of the
617 Sierra Nevada, USA. *Ecological Applications* **0**, e01902 (2019).
- 618 10. USDAFS. Press Release: Record 129 million dead trees in California. [https://www.fs.usda.gov/Internet](https://www.fs.usda.gov/Internet/FSE_DOCUMENTS/fseprd566303.pdf)
619 /FSE_DOCUMENTS/fseprd566303.pdf (2017).
- 620 11. Young, D. J. N. *et al.* Long-term climate and competition explain forest mortality patterns under extreme
621 drought. *Ecology Letters* **20**, 78–86 (2017).
- 622 12. Raffa, K. F. *et al.* Cross-scale drivers of natural disturbances prone to anthropogenic amplification: The
623 dynamics of bark beetle eruptions. *BioScience* **58**, 501–517 (2008).
- 624 13. Boone, C. K., Aukema, B. H., Bohlmann, J., Carroll, A. L. & Raffa, K. F. Efficacy of tree defense
625 physiology varies with bark beetle population density: A basis for positive feedback in eruptive species. *Can.*
626 *J. For. Res.* **41**, 1174–1188 (2011).

- 627 14. Fettig, C. J., Mortenson, L. A., Bulaon, B. M. & Foulk, P. B. Tree mortality following drought in the
628 central and southern Sierra Nevada, California, U.S. *Forest Ecology and Management* **432**, 164–178 (2019).
- 629 15. Stephenson, N. L., Das, A. J., Ampersee, N. J. & Bulaon, B. M. Which trees die during drought? The
630 key role of insect host-tree selection. *Journal of Ecology* **75**, 2383–2401 (2019).
- 631 16. Senf, C., Campbell, E. M., Pflugmacher, D., Wulder, M. A. & Hostert, P. A multi-scale analysis of
632 western spruce budworm outbreak dynamics. *Landscape Ecol* **32**, 501–514 (2017).
- 633 17. Seidl, R. *et al.* Small beetle, large-scale drivers: How regional and landscape factors affect outbreaks of
634 the European spruce bark beetle. *J Appl Ecol* **53**, 530–540 (2016).
- 635 18. Fettig, C. J. Native bark beetles and wood borers in Mediterranean forests of California. in *Insects and*
636 *diseases of Mediterranean Forest systems* 499–528 (Springer International Publishing, 2016).
- 637 19. Raffa, K. F. & Berryman, A. A. The role of host plant resistance in the colonization behavior and ecology
638 of bark beetles (Coleoptera: Scolytidae). *Ecological Monographs* **53**, 27–49 (1983).
- 639 20. Logan, J. A., White, P., Bentz, B. J. & Powell, J. A. Model analysis of spatial patterns in mountain pine
640 beetle outbreaks. *Theoretical Population Biology* **53**, 236–255 (1998).
- 641 21. Wallin, K. F. & Raffa, K. F. Feedback between individual host selection behavior and population dynamics
642 in an eruptive herbivore. *Ecological Monographs* **74**, 101–116 (2004).
- 643 22. Franceschi, V. R., Krokene, P., Christiansen, E. & Krekling, T. Anatomical and chemical defenses of
644 conifer bark against bark beetles and other pests. *New Phytologist* **167**, 353–376 (2005).
- 645 23. Raffa, K. F., Grégoire, J.-C. & Staffan Lindgren, B. Natural history and ecology of bark beetles. in *Bark*
646 *Beetles* 1–40 (Elsevier, 2015). doi:10.1016/B978-0-12-417156-5.00001-0.
- 647 24. Bentz, B. J. *et al.* Climate change and bark beetles of the western United States and Canada: Direct and
648 indirect effects. *BioScience* **60**, 602–613 (2010).
- 649 25. DeRose, R. J. & Long, J. N. Drought-driven disturbance history characterizes a southern Rocky Mountain
650 subalpine forest. *Can. J. For. Res.* **42**, 1649–1660 (2012).
- 651 26. Hart, S. J., Veblen, T. T., Schneider, D. & Molotch, N. P. Summer and winter drought drive the initiation
652 and spread of spruce beetle outbreak. *Ecology* **98**, 2698–2707 (2017).
- 653 27. Netherer, S., Panassiti, B., Pennerstorfer, J. & Matthews, B. Acute drought Is an important driver of
654 bark beetle infestation in Austrian Norway spruce stands. *Front. For. Glob. Change* **2**, (2019).

- 655 28. Kaiser, K. E., McGlynn, B. L. & Emanuel, R. E. Ecohydrology of an outbreak: Mountain pine beetle
656 impacts trees in drier landscape positions first. *Ecohydrology* **6**, 444–454 (2013).
- 657 29. Marini, L. *et al.* Climate drivers of bark beetle outbreak dynamics in Norway spruce forests. *Ecography*
658 **40**, 1426–1435 (2017).
- 659 30. Sambaraju, K. R., Carroll, A. L. & Aukema, B. H. Multiyear weather anomalies associated with range
660 shifts by the mountain pine beetle preceding large epidemics. *Forest Ecology and Management* **438**, 86–95
661 (2019).
- 662 31. Hayes, C. J., Fettig, C. J. & Merrill, L. D. Evaluation of multiple funnel traps and stand characteristics
663 for estimating western pine beetle-caused tree mortality. *Journal of Economic Entomology* **102**, 2170–2182
664 (2009).
- 665 32. Thistle, H. W. *et al.* Surrogate pheromone plumes in three forest trunk spaces: Composite statistics and
666 case studies. *Forest Science* **50**, (2004).
- 667 33. Miller, J. M. & Keen, F. P. *Biology and control of the western pine beetle: A summary of the first fifty*
668 *years of research.* (US Department of Agriculture, 1960).
- 669 34. Chubaty, A. M., Roitberg, B. D. & Li, C. A dynamic host selection model for mountain pine beetle,
670 *Dendroctonus ponderosae* Hopkins. *Ecological Modelling* **220**, 1241–1250 (2009).
- 671 35. Graf, M., Reid, M. L., Aukema, B. H. & Lindgren, B. S. Association of tree diameter with body size and
672 lipid content of mountain pine beetles. *The Canadian Entomologist* **144**, 467–477 (2012).
- 673 36. Geiszler, D. R. & Gara, R. I. Mountain pine beetle attack dynamics in lodgepole pine. in *Theory and*
674 *Practice of Mountain Pine Beetle Management in Lodgepole Pine Forests: Symposium Proceedings.* A. A.
675 *Berryman, G. D. Amman and R. W. Stark (Eds)* (1978).
- 676 37. Klein, W. H., Parker, D. L. & Jensen, C. E. Attack, emergence, and stand depletion trends of the
677 mountain pine beetle in a lodgepole pine stand during an outbreak. *Environ Entomol* **7**, 732–737 (1978).
- 678 38. Mitchell, R. G. & Preisler, H. K. Analysis of spatial patterns of lodgepole pine attacked by outbreak
679 populations of the mountain pine beetle. *Forest Science* **37**, 1390–1408 (1991).
- 680 39. Preisler, H. K. Modelling spatial patterns of trees attacked by bark-beetles. *Applied Statistics* **42**, 501
681 (1993).
- 682 40. Jactel, H. & Brockerhoff, E. G. Tree diversity reduces herbivory by forest insects. *Ecology Letters* **10**,
683 835–848 (2007).

- 684 41. Faccoli, M. & Bernardinelli, I. Composition and elevation of spruce forests affect susceptibility to bark
685 beetle attacks: Implications for forest management. *Forests* **5**, 88–102 (2014).
- 686 42. Berryman, A. A. Population dynamics of bark beetles. in *Bark Beetles in North American Conifers: A*
687 *System for the Study of Evolutionary Biology* 264–314 (1982).
- 688 43. Fettig, C. J. *et al.* The effectiveness of vegetation management practices for prevention and control of
689 bark beetle infestations in coniferous forests of the western and southern United States. *Forest Ecology and*
690 *Management* **238**, 24–53 (2007).
- 691 44. Moeck, H. A., Wood, D. L. & Lindahl, K. Q. Host selection behavior of bark beetles (Coleoptera:
692 Scolytidae) attacking *Pinus ponderosa*, with special emphasis on the western pine beetle, *Dendroctonus*
693 *brevicomis*. *Journal of Chemical Ecology* **7**, 49–83 (1981).
- 694 45. Evenden, M. L., Whitehouse, C. M. & Sykes, J. Factors influencing flight capacity of the mountain pine
695 beetle (Coleoptera: Curculionidae: Scolytinae). *Environ Entomol* **43**, 187–196 (2014).
- 696 46. Raffa, K. F. & Berryman, A. A. Accumulation of monoterpenes and associated volatiles following
697 inoculation of grand fir with a fungus transmitted by the fir engraver, *Scolytus ventralis* (Coleoptera:
698 Scolytidae). *The Canadian Entomologist* **114**, 797–810 (1982).
- 699 47. Anderegg, W. R. L. *et al.* Tree mortality from drought, insects, and their interactions in a changing
700 climate. *New Phytologist* **208**, 674–683 (2015).
- 701 48. Kane, V. R. *et al.* Assessing fire effects on forest spatial structure using a fusion of Landsat and airborne
702 LiDAR data in Yosemite National Park. *Remote Sensing of Environment* **151**, 89–101 (2014).
- 703 49. Larson, A. J. & Churchill, D. Tree spatial patterns in fire-frequent forests of western North America,
704 including mechanisms of pattern formation and implications for designing fuel reduction and restoration
705 treatments. *Forest Ecology and Management* **267**, 74–92 (2012).
- 706 50. Morris, J. L. *et al.* Managing bark beetle impacts on ecosystems and society: Priority questions to
707 motivate future research. *Journal of Applied Ecology* **54**, 750–760 (2017).
- 708 51. Shiklomanov, A. N. *et al.* Enhancing global change experiments through integration of remote-sensing
709 techniques. *Frontiers in Ecology and the Environment* **0**, (2019).
- 710 52. Jeronimo, S. M. A. *et al.* Forest structure and pattern vary by climate and landform across active-fire
711 landscapes in the montane Sierra Nevada. *Forest Ecology and Management* **437**, 70–86 (2019).
- 712 53. Roussel, J.-R., Auty, D., De Boissieu, F. & Meador, A. S. *lidR: Airborne LiDAR data manipulation and*

- 713 *visualization for forestry applications*. (2019).
- 714 54. McDowell, N. *et al.* Mechanisms of plant survival and mortality during drought: Why do some plants
715 survive while others succumb to drought? *New Phytologist* **178**, 719–739 (2008).
- 716 55. Seybold, S. J. *et al.* Management of western North American bark beetles with semiochemicals. *Annual*
717 *Review of Entomology* **63**, 407–432 (2018).
- 718 56. Fettig, C. J., McKelvey, S. R. & Huber, D. P. W. Nonhost angiosperm volatiles and Verbenone disrupt
719 response of western pine beetle, *Dendroctonus brevicomis* (Coleoptera: Scolytidae), to attractant-baited traps.
720 *ecen* **98**, 2041–2048 (2005).
- 721 57. Fettig, C. J., Dabney, C. P., McKelvey, S. R. & Huber, D. P. W. Nonhost angiosperm volatiles and
722 verbenone protect individual ponderosa pines from attack by western pine beetle and red turpentine beetle
723 (Coleoptera: Curculionidae, Scolytinae). *west j appl for* **23**, 40–45 (2008).
- 724 58. Fettig, C. J. *et al.* Efficacy of ‘Verbenone Plus’ for protecting ponderosa pine trees and stands from
725 *Dendroctonus brevicomis* (Coleoptera: Curculionidae) attack in British Columbia and California. *J Econ*
726 *Entomol* **105**, 1668–1680 (2012).
- 727 59. Oliver, W. W. Is self-thinning in ponderosa pine ruled by *Dendroctonus* bark beetles? in *Forest health*
728 *through silviculture: Proceedings of the 1995 National Silviculture Workshop* 6 (1995).
- 729 60. Fettig, C. & McKelvey, S. Resiliency of an Interior Ponderosa Pine Forest to Bark Beetle Infestations
730 Following Fuel-Reduction and Forest-Restoration Treatments. *Forests* **5**, 153–176 (2014).
- 731 61. Fettig, C. J. & Hilszczański, J. Management strategies for bark beetles in conifer forests. in *Bark Beetles*
732 555–584 (Elsevier, 2015). doi:10.1016/B978-0-12-417156-5.00014-9.
- 733 62. Chesson, P. Mechanisms of maintenance of species diversity. *Annual Review of Ecology and Systematics*
734 **31**, 343–366 (2000).
- 735 63. Fricker, G. A. *et al.* More than climate? Predictors of tree canopy height vary with scale in complex
736 terrain, Sierra Nevada, CA (USA). *Forest Ecology and Management* **434**, 142–153 (2019).
- 737 64. Ma, S., Concilio, A., Oakley, B., North, M. & Chen, J. Spatial variability in microclimate in a mixed-conifer
738 forest before and after thinning and burning treatments. *Forest Ecology and Management* **259**, 904–915
739 (2010).
- 740 65. Stovall, A. E. L., Shugart, H. & Yang, X. Tree height explains mortality risk during an intense drought.
741 *Nature Communications* **10**, 1–6 (2019).

- 742 66. Stephenson, N. L. & Das, A. J. Height-related changes in forest composition explain increasing tree
743 mortality with height during an extreme drought. *Nature Communications* **11**, 3402 (2020).
- 744 67. Stovall, A. E. L., Shugart, H. H. & Yang, X. Reply to ‘Height-related changes in forest composition
745 explain increasing tree mortality with height during an extreme drought’. *Nature Communications* **11**, 3401
746 (2020).
- 747 68. Person, H. L. Tree selection by the western pine beetle. *J for* **26**, 564–578 (1928).
- 748 69. Person, H. L. Theory in explanation of the selection of certain trees by the western pine beetle. *J for* **29**,
749 696–699 (1931).
- 750 70. Pile, L. S., Meyer, M. D., Rojas, R., Roe, O. & Smith, M. T. Drought impacts and compounding mortality
751 on forest trees in the southern Sierra Nevada. *Forests* **10**, 237 (2019).
- 752 71. Frey, J., Kovach, K., Stemmler, S. & Koch, B. UAV photogrammetry of forests as a vulnerable process.
753 A sensitivity analysis for a structure from motion RGB-image pipeline. *Remote Sensing* **10**, 912 (2018).
- 754 72. James, M. R. & Robson, S. Mitigating systematic error in topographic models derived from UAV and
755 ground-based image networks. *Earth Surface Processes and Landforms* **39**, 1413–1420 (2014).
- 756 73. Gray, P. C. *et al.* A convolutional neural network for detecting sea turtles in drone imagery. *Methods in*
757 *Ecology and Evolution* **10**, 345–355 (2019).
- 758 74. Millar, C. I., Stephenson, N. L. & Stephens, S. L. Climate change and forests of the future: Managing in
759 the face of uncertainty. *Ecological Applications* **17**, 2145–2151 (2007).
- 760 75. Vose, J. M. *et al.* *Forests. In Impacts, Risks, and Adaptation in the United States: The Fourth National*
761 *Climate Assessment, Volume II [Reidmiller, D. R., C. W. Avery, D. R. Easterling, K. E. Kunkel, K. L. M.*
762 *Lewis, T. K. Maycock, and B. C. Stewart (eds.)].* 232–267 <https://nca2018.globalchange.gov/chapter/6/>
763 (2018) doi:10.7930/NCA4.2018.CH6.
- 764 76. Bedard, W. D. *et al.* Western pine beetle: Field response to its sex pheromone and a synergistic host
765 terpene, myrcene. *Science* **164**, 1284–1285 (1969).
- 766 77. Byers, J. A. & Wood, D. L. Interspecific inhibition of the response of the bark beetles, *Dendroctonus*
767 *brevicomis* and *Ips paraconfusus*, to their pheromones in the field. *J Chem Ecol* **6**, 149–164 (1980).
- 768 78. Shepherd, W. P., Huber, D. P. W., Seybold, S. J. & Fettig, C. J. Antennal responses of the western pine
769 beetle, *Dendroctonus brevicomis* (Coleoptera: Curculionidae), to stem volatiles of its primary host, *Pinus*
770 *ponderosa*, and nine sympatric nonhost angiosperms and conifers. *Chemoecology* **17**, 209–221 (2007).

- 771 79. DJI. Zenmuse X3 - Creativity Unleashed. *DJI Official* <https://www.dji.com/zenmuse-x3/info> (2015).
- 772 80. Micasense. MicaSense. [https://support.micasense.com/hc/en-us/articles/215261448-RedEdge-User-](https://support.micasense.com/hc/en-us/articles/215261448-RedEdge-User-Manual-PDF-Download-)
773 [Manual-PDF-Download-](https://support.micasense.com/hc/en-us/articles/215261448-RedEdge-User-Manual-PDF-Download-) (2015).
- 774 81. DJI. DJI - The World Leader in Camera Drones/Quadcopters for Aerial Photography. *DJI Official*
775 <https://www.dji.com/matrice100/info> (2015).
- 776 82. Wyngaard, J. *et al.* Emergent challenges for science sUAS data management: Fairness through community
777 engagement and best practices development. *Remote Sensing* **11**, 1797 (2019).
- 778 83. Rouse, W., Haas, R. H., Deering, W. & Schell, J. A. *Monitoring the vernal advancement and retrogradation*
779 *(green wave effect) of natural vegetation.* (1973).
- 780 84. DronesMadeEasy. Map Pilot for DJI on iOS. *App Store* [https://itunes.apple.com/us/app/map-pilot-for-](https://itunes.apple.com/us/app/map-pilot-for-dji/id1014765000?mt=8)
781 [dji/id1014765000?mt=8](https://itunes.apple.com/us/app/map-pilot-for-dji/id1014765000?mt=8) (2018).
- 782 85. Farr, T. G. *et al.* The shuttle radar topography mission. *Reviews of Geophysics* **45**, (2007).
- 783 86. Zhang, W. *et al.* An easy-to-use airborne LiDAR data filtering method based on cloth simulation. *Remote*
784 *Sensing* **8**, 501 (2016).
- 785 87. Hijmans, R. J. *et al.* *Raster: Geographic data analysis and modeling.* (2019).
- 786 88. Gitelson, A. & Merzlyak, M. N. Spectral reflectance changes associated with autumn senescence of
787 *Aesculus hippocastanum* L. And *Acer platanoides* L. Leaves. Spectral features and relation to chlorophyll
788 estimation. *Journal of Plant Physiology* **143**, 286–292 (1994).
- 789 89. Coops, N. C., Johnson, M., Wulder, M. A. & White, J. C. Assessment of QuickBird high spatial resolution
790 imagery to detect red attack damage due to mountain pine beetle infestation. *Remote Sensing of Environment*
791 **103**, 67–80 (2006).
- 792 90. Clevers, J. G. P. W. & Gitelson, A. A. Remote estimation of crop and grass chlorophyll and nitrogen
793 content using red-edge bands on Sentinel-2 and -3. *International Journal of Applied Earth Observation and*
794 *Geoinformation* **23**, 344–351 (2013).
- 795 91. Li, W., Guo, Q., Jakubowski, M. K. & Kelly, M. A new method for segmenting individual trees from the
796 LiDAR point cloud. *Photogrammetric Engineering & Remote Sensing* **78**, 75–84 (2012).
- 797 92. Jakubowski, M. K., Li, W., Guo, Q. & Kelly, M. Delineating individual trees from LiDAR data: A
798 comparison of vector- and raster-based segmentation approaches. *Remote Sensing* **5**, 4163–4186 (2013).

- 799 93. Shin, P., Sankey, T., Moore, M. & Thode, A. Evaluating unmanned aerial vehicle images for estimating
800 forest canopy fuels in a ponderosa pine stand. *Remote Sensing* **10**, 1266 (2018).
- 801 94. Roussel, J.-R. *lidRplugins: Extra functions and algorithms for lidR package.* (2019).
- 802 95. Eysn, L. *et al.* A benchmark of LiDAR-based single tree detection methods using heterogeneous forest
803 data from the alpine space. *Forests* **6**, 1721–1747 (2015).
- 804 96. Vega, C. *et al.* PTrees: A point-based approach to forest tree extraction from LiDAR data. *International*
805 *Journal of Applied Earth Observation and Geoinformation* **33**, 98–108 (2014).
- 806 97. Plowright, A. *ForestTools: Analyzing remotely sensed forest data.* (2018).
- 807 98. Pau, G., Fuchs, F., Sklyar, O., Boutros, M. & Huber, W. EBImage: An R package for image processing
808 with applications to cellular phenotypes. *Bioinformatics* **26**, 979–981 (2010).
- 809 99. Meyer, F. & Beucher, S. Morphological segmentation. *Journal of Visual Communication and Image*
810 *Representation* **1**, 21–46 (1990).
- 811 100. Hunziker, P. *Velox: Fast raster manipulation and extraction.* (2017).
- 812 101. Kuhn, M. Building predictive models in R using the caret package. *Journal of Statistical Software* **28**,
813 1–26 (2008).
- 814 102. Wang, Y. *et al.* Is field-measured tree height as reliable as believed A comparison study of tree height
815 estimates from field measurement, airborne laser scanning and terrestrial laser scanning in a boreal forest.
816 *ISPRS Journal of Photogrammetry and Remote Sensing* **147**, 132–145 (2019).
- 817 103. Stephenson, N. Actual evapotranspiration and deficit: Biologically meaningful correlates of vegetation
818 distribution across spatial scales. *Journal of Biogeography* **25**, 855–870 (1998).
- 819 104. Flint, L. E., Flint, A. L., Thorne, J. H. & Boynton, R. Fine-scale hydrologic modeling for regional
820 landscape applications: The California Basin Characterization Model development and performance. *Ecological*
821 *Processes* **2**, 25 (2013).
- 822 105. Millar, C. I. *et al.* Forest mortality in high-elevation whitebark pine (*Pinus albicaulis*) forests of eastern
823 California, USA: Influence of environmental context, bark beetles, climatic water deficit, and warming.
824 *Canadian Journal of Forest Research* **42**, 749–765 (2012).
- 825 106. Baldwin, B. G. *et al.* Species richness and endemism in the native flora of California. *American Journal*
826 *of Botany* **104**, 487–501 (2017).

- 827 107. Bürkner, P.-C. **brms**: An *R* package for bayesian multilevel models using *Stan*. *Journal of Statistical*
828 *Software* **80**, 1–28 (2017).
- 829 108. Hoffman, M. D. & Gelman, A. The No-U-Turn Sampler: Adaptively setting path lengths in Hamiltonian
830 Monte Carlo. *Journal of Machine Learning Research* **15**, 31 (2014).
- 831 109. Carpenter, B. *et al.* Stan: A Probabilistic Programming Language. *Journal of Statistical Software* **76**,
832 1–32 (2017).
- 833 110. Brooks, S. P. & Gelman, A. General methods for monitoring convergence of iterative simulations.
834 *Journal of Computational and Graphical Statistics* **7**, 434 (1998).
- 835 111. Gabry, J., Simpson, D., Vehtari, A., Betancourt, M. & Gelman, A. Visualization in Bayesian workflow.
836 *Journal of the Royal Statistical Society: Series A (Statistics in Society)* **182**, 389–402 (2019).
- 837 112. Koontz, M. J., Latimer, A. M., Mortenson, L. A., Fettig, C. J. & North, M. P. Drone-derived data
838 supporting "Cross-scale interaction of host tree size and climatic water deficit governs bark beetle-induced
839 tree mortality". (2020) doi:10.17605/OSF.IO/3CWF9.
- 840 113. Baldwin, B. G. *et al.* Master spatial file for native California vascular plants used by Baldwin *et al.*
841 (2017 Amer. J. Bot.). *American Journal of Botany* **3** (2017).
- 842 114. R Core Team. *R: A language and environment for statistical computing*. (R Foundation for Statistical
843 Computing, 2018).
- 844 115. Koontz, M. J., Latimer, A. M., Mortenson, L. A., Fettig, C. J. & North, M. P. Local-structure-wpb-
845 severity. (2019) doi:10.17605/OSF.IO/WPK5Z.